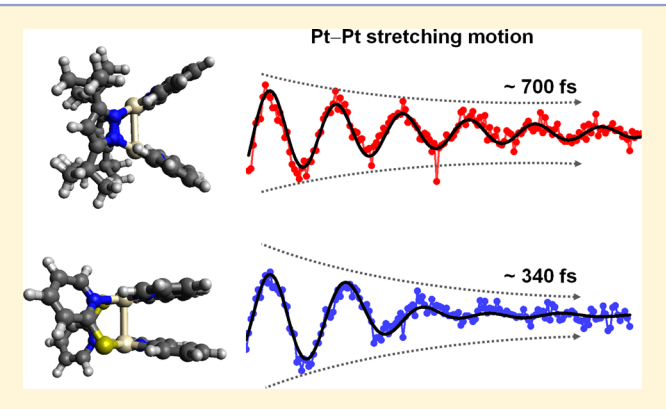


# Coherent Vibrational Wavepacket Dynamics in Platinum(II) Dimers and Their Implications

Pyosang Kim,<sup>†,‡</sup> Matthew S. Kelley,<sup>‡</sup> Arnab Chakraborty,<sup>§</sup> Nolan L. Wong,<sup>‡</sup> Richard P. Van Duyne,<sup>‡</sup> George C. Schatz,\*,<sup>‡</sup> Felix N. Castellano,\*,<sup>§</sup> and Lin X. Chen\*,<sup>†,‡</sup>

Supporting Information

ABSTRACT: Vibrational coherence in the metal-metal-toligand-charge transfer (MMLCT) excited state of cyclometalated platinum dimers with a pseudo  $C_2$  symmetry was investigated where two nearly degenerate transitions from the highest occupied molecular orbital (metal-metal  $\sigma^*$  orbital) to higher energy ligand  $\pi^*$  orbitals could be simultaneously induced. We observed oscillatory features in femtosecond degenerate transient absorption (TA) signals from complexes  $[(ppy)Pt(\mu^{-t}Bu_2pz)]_2$ (1) and anti-[(ppy)Pt( $\mu$ -pyt)], (2), which are attributed to coherent nuclear motions that modulate the HOMO (antibonding  $\sigma^*$ ) energy level, and hence, the energy for the MMLCT transition. The characteristics of such coherent nuclear motions, such as the oscillatory frequency and the dephasing time, differ between 1 and 2 and are explained by mainly two structural



factors that could influence the vibrational coherence: the Pt-Pt distance (2.97 Å for 1 vs 2.85 Å for 2) and molecular shape (1 in an "A" frame vs 2 in an "H" frame). Because the electronic coupling between the two Pt atoms determines the energy splitting of the bonding  $\sigma$  and antibonding  $\sigma^*$  orbital, the Pt-Pt stretching mode coupled to the MMLCT transition changes the inter Pt distance from that of the ground state. Interestingly, while 1 shows a single Pt-Pt stretching frequency of 120 cm-1 in the MMLCT state, 2 exhibits multiple downshifted frequencies (80 and 105 cm<sup>-1</sup>) in the MMLCT state along with a shorter vibrational dephasing time than I. Based on the ground state optimized structures and Raman calculations, the changes evident in the vibrational wavepacket dynamics in 2 are closely correlated with the "H" framed geometry in 2 compared to the "A" frame in 1, leading to the sharp increase in  $\pi - \pi$  interaction between ppy ligands. Although the TA experiments do not directly reveal the ultrafast intersystem crossing (ISC) because of a strong coherent spike at early time scales, the dependence of the vibrational wavepacket dynamics on molecular geometry can be understood based on previously proposed potential energy surfaces as a function of Pt-Pt distance, suggesting that the interaction between the cyclometalating ligands can be a key factor in determining the Pt-Pt shortening and the related energy relaxation dynamics in the Pt(II) dimers. Further experiments using femtosecond broadband TA and X-ray scattering spectroscopy are planned to investigate directly the ISC and Pt-Pt contraction to support the relationship between ground state molecular geometry and photoinduced structural changes in the Pt(II) dimers.

# ■ INTRODUCTION

Luminescent platinum(II) complexes have generated research interest for their application as phosphorescent materials in organic light-emitting diodes (OLEDs) due to their high quantum efficiency.<sup>1–4</sup> Mononuclear platinum complexes can exhibit specific luminescence properties when they selfassemble into arrays or supramolecular architectures, stemming from  $\pi - \pi$  stacking between aromatic ligands coordinated with platinum. 5-9 However, these features are often difficult to control with well-defined structures and to reproduce in different environments (e.g., concentration, solvent, and temperature). In comparison, dimeric Pt(II) complexes are very attractive systems with well-defined Pt-Pt distances in a

covalently linked frame. In the past several years, Ma and Thompson, Castellano et al., and later Ma and co-workers have reported multiple series of cyclometalated platinum(II) dimer complexes with pyrazolate (pz) bridges (such as  $Pt(ppy)(\mu$ - $[R_2pz]_2$  with R= H, CH<sub>3</sub>, phenyl, and t-butyl), which have variable Pt-Pt distances controlled by the bulkiness of the groups at the 3- and 5- positions of the pyrazolate bridge. 10-14 Steric hindrance from the bulkier groups in the pyrazolate

Special Issue: Prashant V. Kamat Festschrift

Received: February 15, 2018 Revised: April 23, 2018 Published: April 27, 2018

<sup>&</sup>lt;sup>†</sup>Chemical Science and Engineering Division, Argonne National Laboratory, Lemont, Illinois 60439, United States

<sup>\*</sup>Department of Chemistry, Northwestern University, Evanston, Illinois 60208, United States

<sup>§</sup>Department of Chemistry, North Carolina State University, Raleigh, North Carolina 27695-8204, United States

Scheme 1. Molecular Structures of 1 ([(ppy)Pt( $\mu$ - $^t$ Bu<sub>2</sub>pz)]<sub>2</sub>) and 2 (anti-[(ppy)Pt( $\mu$ -pyt)]<sub>2</sub>)

bridge can act as a tweezer, forcing shorter the P—Pt distances. This effect results in significantly red-shifted absorption and emission features compared to those of corresponding monomeric Pt complexes.

Monomeric square planar Pt(II) complexes typically exhibit a mixture of ligand centered (LC) and metal-to-ligand charge transfer (MLCT) transitions. However, the nature of the electronic transitions in dimeric Pt-Pt complexes depends on the electronic coupling via the Pt-Pt interaction, which causes energy splitting between the bonding  $\sigma$  and antibonding  $\sigma^*$ molecular orbitals (MOs) formed by the two the two 5d<sub>z</sub><sup>2</sup> orbitals. In these dimer complexes, as the Pt-Pt distance shortens, the  $\sigma$ - $\sigma$ \* energy split increases, causing the HOMO energy to rise. The lowest energy transition in the dimers thus switches from the LC/MLCT to the metal-metal-to-ligand charge transfer (MMLCT) transitions, i.e.,  $\sigma^*(Pt_2) \to \pi^*(ppy)$ . Such a MMLCT transition depletes an antibonding electron in a  $\sigma^*(Pt_2)$  MO and hence increases the Pt-Pt bond order by 0.5, resulting in a contraction of the Pt-Pt bond. Similar Pt-Pt shortenings have also been found in  $[Pt_2(pop)_4]^{4-}$  (pop =  $\mu$ pyrophosphite-P,P') complexes, and the shortening has been observed by time-resolved X-ray diffraction, <sup>15</sup> solution-state scattering, <sup>16,17</sup> and extended X-ray absorption fine structure (EXAFS) spectroscopy. 16,18-21

In several recent studies, molecular "butterfly" motions in these pz bridged complexes have been suggested based on direct structural measurements in solution X-ray scattering of the MMLCT state<sup>22</sup> and on a dual emission dependent on the temperature and viscosity of the environment. These motions originate from a thermalized excited state equilibrium between two energy minima on the triplet excited-state potential energy surface (PES), a <sup>3</sup>LC/MLCT and a <sup>3</sup>MMLCT state. <sup>11,13</sup> Theoretical calculations also support this hypothesis. <sup>23,24</sup> However, these previous studies cannot unravel structural dynamics along the excited state surface due to a lack of experimental time resolution, although the relevant knowledge of the relationship between molecular geometry and dynamics is indispensable to understand the photophysical properties of cyclometalated Pt(II) dimers.

Previously, coherent wavepacket motions were characterized in the platinum diphosphate complex  $[Pt_2(pop)_4]^{4-}$  by several studies using pump–probe absorption/emission spectroscopy, which showed a coherent Pt–Pt stretch vibration of increased frequency on the singlet  $^1A_{2u}$   $(d\sigma^* \to p\sigma)$  excited state compared to that of the ground state.  $^{18,19,25-27}$  Such an observation is agreeable with Pt–Pt bond formation or contraction in the excited state.  $^{26,27}$  Although  $[Pt_2(pop)_4]^{4-}$  shares similar structural distortion in the excited state with the

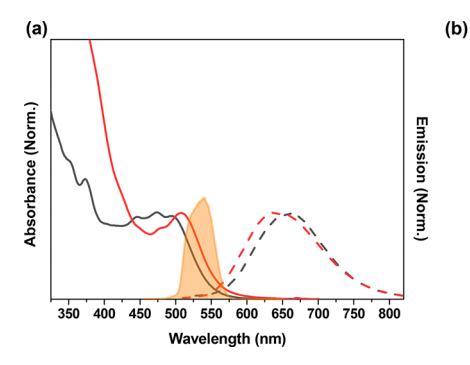
cyclometalated Pt(II) dimers, coherent nuclear dynamics are expected to have a totally different origin because the MLCT and MMLCT transitions are absent in  $[Pt_2(pop)_4]^{4-}$ .

Because the lowest energy electronic transitions (LC/MLCT or the MMLCT) in the Pt-Pt dimer are sensitive to the electronic coupling between the two Pt centers as described earlier, the vibrational motions that alter this distance could also alter electronic coupling and electronic coherence as shown in recent calculations<sup>28</sup> and hence the excited state pathways. In order to reveal and prove the possibility of vibrationally modulated electronic transitions and the influence of vibrational coherence on excited state pathway, we will first detect nuclear coherence in the excited state and their correlations with molecular structural factors. Using femtosecond degenerate transient absorption spectroscopy, we report the results from our investigation of the coherent vibrational wavepacket dynamics in the MMLCT excited state of Pt(II) dimers and their correlations with the key structural element, the ground state Pt-Pt distance. Comparative studies of coherent nuclear dynamics have been carried out for two cyclometalated Pt(II) dimers bridged by different ligands,  $[(ppy)Pt(\mu-tBu_2pz)]_2$  (1) and  $anti-[(ppy)Pt(\mu-pyt)]_2$  (pyt = pyridine-2-thiol) (2) (Scheme 1). Based on the X-ray crystal structures, 2 shows an "H"-frame dimeric structure in contrast to the "A"-frame geometry of 1 owing to 4-bond-bridging ligands.<sup>29</sup> Furthermore, pyt bridging ligand results in a shorter Pt-Pt distance in the ground state despite the absence of bulky substituents such as  ${}^{t}$ Bu groups on the bridging ligands, resulting in 2.849 Å for 2 compared to 2.97 Å for 1.  ${}^{29,30}$  The observation of totally distinct coherent wavepacket dynamics between 1 and 2 presented here provides crucial information about the correlation between molecular geometry and energy relaxation dynamics, supported by complementary quantum chemical calculations, which successfully clarify the origin of coherent nuclear dynamics.

#### EXPERIMENTAL SECTION

**Sample Preparation.** Complex **1** was available from previous studies. Complex **2** was prepared as previously described by Kato and co-workers with a <sup>1</sup>H NMR spectrum and single crystal X-ray structure consistent with the single isomer *anti*-configuration.

**Steady-state Measurements.** Steady-state absorption spectra were measured with a Shimadzu UV-3600 UV-vis-NIR spectrophotometer. Steady-state emission spectra were collected with a Horiba Scientific model Fluorolog-3 spectrometer. Both measurements were carried out in 1 cm optical glass cuvettes at room temperature.



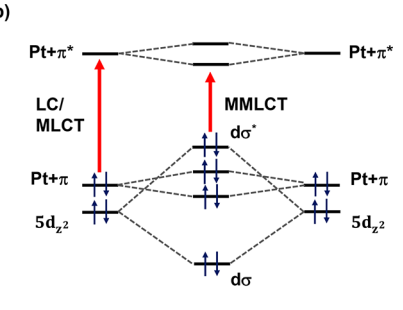


Figure 1. (a) Steady-state absorption (solid line) and emission spectra (dotted line) for 1 (black) and 2 (red) in THF at room temperature. The spectral profile of the laser pulse is also pictured (orange). (b) Qualitative molecular orbital energy diagram.

Femtosecond Degenerate Transient Absorption Measurement. Femtosecond degenerate transient absorption (TA) experiments were performed using a diffractive opticsbased two-dimensional electronic spectroscopic setup. Briefly, the 800 nm pulses of 35 fs duration generated from a 10 kHz regenerative amplified Ti:sapphire laser (Solstice Ace, Spectra-Physics) pumped a home-built visible noncollinear optical parametric amplifier (vis-NOPA). The vis-NOPA output pulse at 535 nm with an ~50 nm bandwidth was compressed by a prism compressor and then split by a 50% beam splitter. The compressed two beams were focused on a diffractive optic (Holoeye) to generate four beams arranged in the BOXCARS geometry, and four beams were then collimated using a 25 cm curve mirror. For TA measurements, the two of four beams were blocked, and the others were used for pump and probe pulses. The pump and probe pulses were focused at the sample position using a 25 cm concave mirror. The time delay between pump and probe beams was varied using a computer controlled motorized translation stage. For the TA spectra, the pump-on and pump-off spectra were obtained by a chopper operating at 200 Hz and detected with a spectrograph (Andor Shamrock) and a CCD camera (Andor Newton). The time resolution of the experiment was determined to be ~30 fs at the sample position from the nonresonant transient grating measurement of MeOH (Figure S1).

The polarization of the pump and probe beams was set by a combination of a half-waveplate and polarizer inserted in both optical paths. The polarization of pump beam in the magicangle TA experiment was set at  $54.7^{\circ}$  to the polarization of probe beam in order to obtain polarization-independent TA decay traces. The parallel  $(I_{\parallel})$  and the perpendicular  $(I_{\perp})$  TA signals were collected independently by changing the polarization of the pump beam to vertical and to horizontal for the polarization of probe beam, respectively. The pump power was 80 nJ at the sample position. All measurements were performed on samples dissolved in degassed solvent (THF and toluene) in 2 mm quartz cuvettes. The concentration was adjusted so that the absorption at the maximum peaks of MMLCT bands was around 0.1.

**Quantum Mechanical Calculations.** Density functional theory (DFT) calculations were performed using ADF 2016.103. For structure optimizations and Raman calculations in the ground state, we used the PBE functional with the zeroth order relativistic approximation (ZORA). A double-zeta polarized basis set (DZP) was used for light atoms, while a triple-zeta basis (TZP) was used for platinum. The platinum core was frozen up to the 4f orbitals.

## RESULTS

Steady-state Spectroscopic Measurements. The steady-state absorption and emission spectra of 1 and 2 in THF are presented in Figure 1a. Based on the previous studies of 1, the lowest energy absorption band with features at 446, 475, and 495 nm (their fine assignments are unclear) is assigned to the MMLCT transitions from the antibonding  $d\sigma^*$ (Pt-Pt) to the  $\pi^*$  (ppy) orbital, and the higher energy absorption band around a peak at 375 nm is attributed to LC/ MLCT transitions. 11 The MMLCT band of 1 is drastically redshifted and intensified in comparison with those complexes of the same molecular frame  $[(ppy)Pt(\mu-R-pz)]_2$  (where R = H, CH<sub>3</sub>, and phenyl-) with less bulky R groups. The red-shift results from the aforementioned "tweezer" effect, resulting in a shorter Pt-Pt distance in the ground state and hence an increased energy splitting of the  $\sigma(5d_{z^2})$  and  $\sigma^*(5d_{z^2})$  MOs, which pushes up the energy of the antibonding HOMO dominated by  $\sigma^*(5d_{\tau^2})$  character (Figure 1b). As the Pt-Pt distance decreases, the lowest energy transitions transform from localized LC/MLCT to MMLCT in nature as the 5d<sub>z</sub><sup>2</sup> orbital overlap from two pseudosymmetric halves of the molecule increases. 11 Such a trend in the absorption/emission spectra also implies that shortening the Pt-Pt distance does not affect the  $\pi^*$  MO energy significantly when the ligands dominating  $\pi^*$  MOs are not in close contact as shown by our previous calculations.<sup>32</sup> Note that 2 has the onset of the red-edge MMLCT bands slightly red-shifted from that of 1.<sup>29</sup> Taking the Pt-Pt distance observed from the ground-state crystal structure (2.97 Å for 1 vs 2.849 Å for 2) into account, <sup>29,30</sup> it is clear that the shorter Pt-Pt distance in 2 would further destabilize the  $d\sigma^*$  energy (Figure 1b). In the emission spectra, both complexes exhibit a broad and featureless spectra with Stokes shifts >4000 cm<sup>-1</sup>, which is attributed to the phosphorescence from the <sup>3</sup>MMLCT state. <sup>11,29</sup> Interestingly, the Stokes shift in 2 is slightly smaller than in 1, suggesting that the two complexes likely undergo structural changes in their MMLCT excited state with different amplitudes.

Coherent Vibrational Wavepacket Motion Detected by Femtosecond Degenerate TA Measurements. To investigate the excited state nuclear vibrational dynamics of 1 and 2, we performed ultrafast degenerate TA measurements. In these measurements, the NOPA spectrum (i.e., 525-560 nm) was set to induce the ground to the MMLCT state transition and launch coherent vibrational motions in the MMLCT state. The TA decay traces at the magic angle  $I(\lambda, t)$  for both complexes at different probe wavelengths  $\lambda$  are shown in Figure 2. The  $I(\lambda, t)$  traces for 1 exhibit weak positive signals until 2 ps in the probe wavelength range, which is consistent with the TA

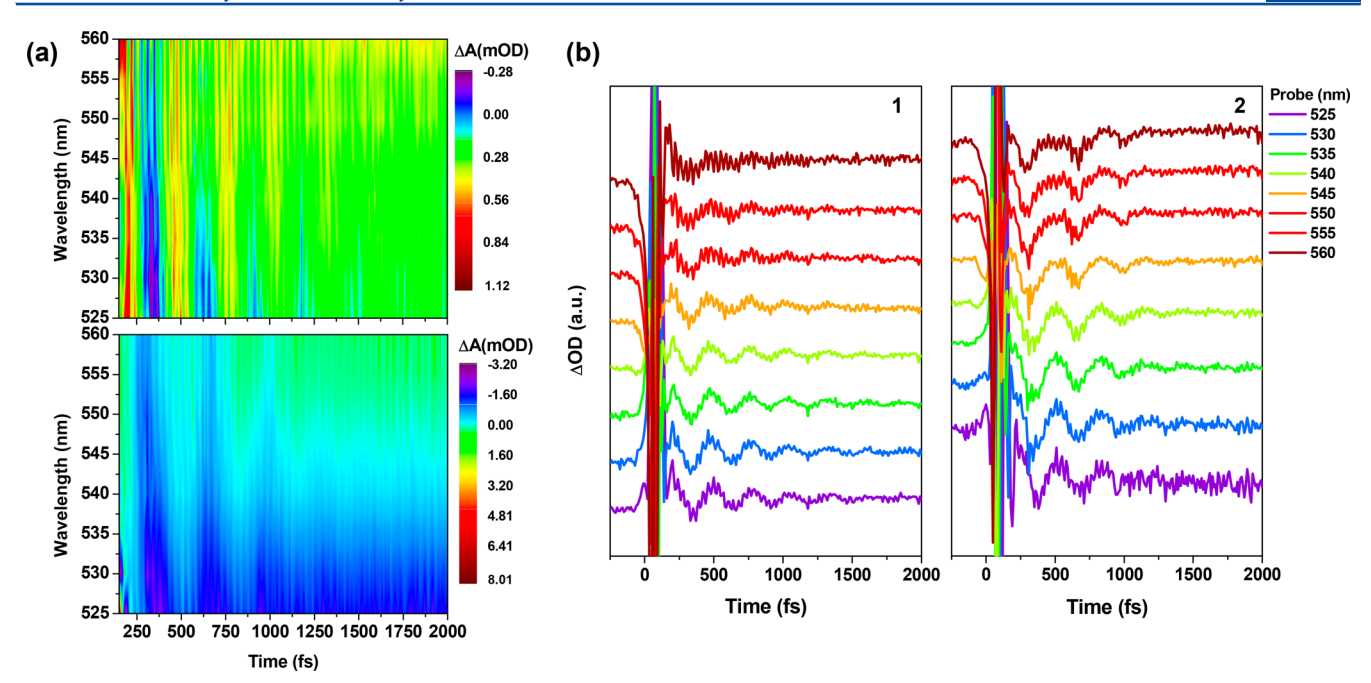


Figure 2. (a) Contour map of degenerate TA data for 1 (top) and 2 (bottom). To show clearly the oscillatory features, the coherent spikes around time zero are omitted. (b) Magic-angle TA kinetics traces at several probe wavelengths for 1 and 2.

spectra obtained earlier with longer pulses (i.e., a IRF, ~200 fs). <sup>32</sup> This previous work also suggested that ultrafast intersystem crossing (ISC) forms the <sup>1</sup>MMLCT to the initial triplet intermediate state within the time resolution of the instrument (i.e., 200 fs). Although the current TA measurements with a ~30 fs IRF should be sufficient to observe the initial signals reflecting the excited state dynamics, the detailed spectral evolution in this ultrafast ISC time window is obscured by a strong coherent spike and oscillatory features around the delay time  $t \approx 0$ . Nevertheless, very strong oscillations beyond the first 100 fs can be revealed up to 2 ps which are attributed to the coherent nuclear motion generated by photoexcitation.

We also obtained magic-angle TA decay  $I(\lambda, t)$  profiles for 2, which show negative signals from  $\lambda = 525$  to 550 nm, while the TA signals above 550 nm convert from negative to positive (Figure 2). Particularly, considering the range above 550 nm is the edge of the ground-state absorption, the observed kinetics traces in those regions originate mainly from stimulated emission (SE) or excited-sate absorption (ESA). To avoid the contributions of the ground-state bleaching (GSB), the time constants of nonoscillatory TA signals are examined at 560 nm by fitting with two exponential functions in a time window from 200 fs to 2 ps. Obviously, the second time constant is too long for the 2 ps experimental time window to obtain an accurate value; hence, we fixed it to a ~500 ps equivalent of a constant offset signal in the experimental data, which is justified considering several hundreds of nanoseconds for the relaxation processes in the triplet state. The fit shows a temporal behavior of the signal with  $\sim$ 600 fs in 1 and  $\sim$ 350 fs in 2, respectively, which are consistent with those in probe wavelength range from 540 to 560 nm (Figure S2). This feature indicates the excited-state dynamics in the early time window (<2 ps) become shorter in going from 1 to 2, though the whole probe range in the current TA is mixed by three signals: GSB, SE, and

Notably, 2 exhibits the strong oscillatory features in the same spectral range as 1 from the coherent nuclear wavepacket

motions. Interestingly, the damping time of I(t) for  ${\bf 2}$  is shorter than that of  ${\bf 1}$ , similar to the trend in the triplet population decay kinetics. Moreover, the I(t) oscillations of  ${\bf 1}$  and  ${\bf 2}$  differ in shape at different probe wavelength, and those in  ${\bf 2}$  at longer probe wavelength (>545 nm) clearly show evidence of more than a single sinusoidal oscillatory signal, which implies that the coherent vibrational wavepacket motions could arise from multiple modes or the anharmonicity in the vibrational potential energy. These vibrational wavepacket dynamics features observed in  ${\bf 2}$  are closely related to its structural factors including the Pt—Pt distance. Detailed and quantified analysis of these coherent oscillatory features are described in the next section.

The coherent vibrational motions in the entire probe wavelength range at the magic angle  $I(\lambda, t)$  differ from our previous study of 1, which reported strong anticorrelated oscillatory features in both the parallel  $I_{\parallel}(t)$  and perpendicular  $I_{\perp}(t)$  TA decay traces, while the magic-angle TA kinetics trace I(t) reconstructed from the equation  $I(t) = [I_{\parallel}(t) + 2I_{\perp}(t)]/3$ had no oscillations.<sup>31</sup> In particular, anticorrelated oscillatory features between and  $I_{\parallel}(t)$  and  $I_{\perp}(t)$  signals were observed. In addition, that study found that the initial anisotropy  $r(t = 0) \approx$ 0.7 indicated a possible electronic coherence between the two pseudo C2-symmetry related and superimposed MMLCT transitions involving the  $\pi^*$  orbitals from the two ppy ligands. Subsequently, quantum mechanical calculations by Li and coworkers demonstrated that the oscillations due to electronic coherence would have a period of 10-20 fs, 10-fold smaller than we observed.<sup>28</sup> Based on this current study, we recognize that the previously observed coherence most likely stems from vibrational wavepacket motions of a Pt-Pt stretch vibrational mode when comparing the results to ground state Raman spectroscopy.31

Using much shorter laser pulses with a corresponding broader excitation spectrum from the vis-NOPA, we performed the TA measurement of 1 in toluene (Figure 3). Instead of reconstructing the magic-angle TA trace from the equation I(t)

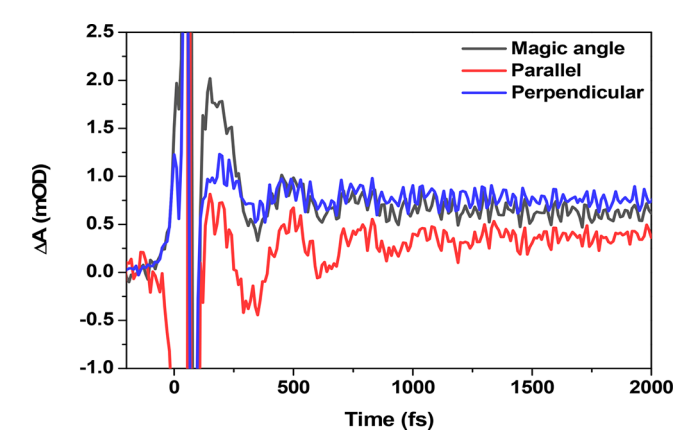


**Figure 3.** Parallel, perpendicular, and magic-angle TA kinetics traces at 535 nm for 1 in toluene at room temperature.

=  $[I_{\parallel}(t) + 2I_{\perp}(t)]/3$ , we directly measured I(t) signals that exhibit oscillatory features. Notably, the lowest frequency oscillation displayed in I(t) remains consistent with that of the same magic-angle TA measurement in THF. Moreover, the oscillations in  $I_{\parallel}(t)$  and  $I_{\perp}(t)$  signals are in phase at the lowest frequency in the directly measured I(t). These results strongly support that the oscillations observed in the TA measurements of 1 are due to coherent vibrational wavepacket motions, rather than electronic coherence. The TA signals in these complexes are extremely weak with  $\Delta OD$  (change in optical density) on the order of  $10^{-3}$ . It was possible that the measurements of  $I_{\parallel}(t)$  and  $I_{\parallel}(t)$  in the previous study using the lock-in detection made it difficult to obtain the absolute phases between the two signals. Figure S3 shows that the oscillatory feature with the lowest frequency has disappeared in the reconstructed TA decay kinetics from the aforementioned equation when the sign of the current  $I_{\parallel}(t)$  is reversed while that of  $I_{\perp}(t)$  remains unchanged. This suggests the flipped sign of  $I_{\parallel}(t)$  in the previous TA anisotropy measurements results in no oscillation in the reconstructed magic-angle TA data.

## Characterization of Vibrational Wavepacket Motions.

The oscillatory components of the TA signals are extracted by subtracting nonoscillatory exponential decay components from the raw TA traces followed by Fourier transform. The Fourier power spectra of 1 and 2 are depicted in Figures 4 and S4. The Fourier power spectra of all complexes show a dominating peak around 100 cm<sup>-1</sup>, independent of the solvents, while the intense peaks at 913 cm<sup>-1</sup> in THF<sup>39</sup> and at 520, 786, and 1006 cm<sup>-1</sup> in toluene 40 are assigned as the solvent peaks. In order to identify relevant vibrational modes and to rationalize the experimentally observed results, we performed structural optimization and a normal-mode analysis for the ground state with DFT calculations, which provide information on the origins of vibrational peaks in the Fourier power spectra in terms of the normal modes as depicted in Figure 5. The experimentally observed intense peaks at 120 cm<sup>-1</sup> in 1 and 105 cm<sup>-1</sup> in 2 (Figure 4) are, respectively, assigned to the Pt-Pt stretching vibrational mode in the MMLCT state, which are in the Raman frequency range for the Pt-Pt stretching normal mode in the ground state (from powder spectra) and those from the calculated frequencies (100 cm<sup>-1</sup> in 1 and 109 cm<sup>-1</sup> in 2). Thus, although the ground state Raman measurements of 1 and 2 are for the solid powder (Figure S5), the results support the assignment of the vibrational wavepacket motions to the Pt-Pt stretching vibration. Considering the significant Pt-Pt distance shortening in the MMLCT state, the above assignment is reasonable and suggestive of a strong coupling of the MMLCT transition with the Pt-Pt stretch vibrational mode. Such an assessment is also supported by the direct observation of Pt-Pt contraction in the triplet <sup>3</sup>MMLCT in the previous transient XAFS (X-ray absorption fine structure)/XANES (Xray absorption near edge structure) studies for 1. 22,30

The coherent vibrational motions in the MMLCT state revealed quantitatively by the Fourier power spectra of the two complexes show distinctly different trends. The differences include: (a) a frequency downshift of the main peak assigned to the Pt–Pt stretching near 100 cm<sup>-1</sup> (compared to that of 1 at 120 cm<sup>-1</sup>) and (b) the involvement of multiple modes. The

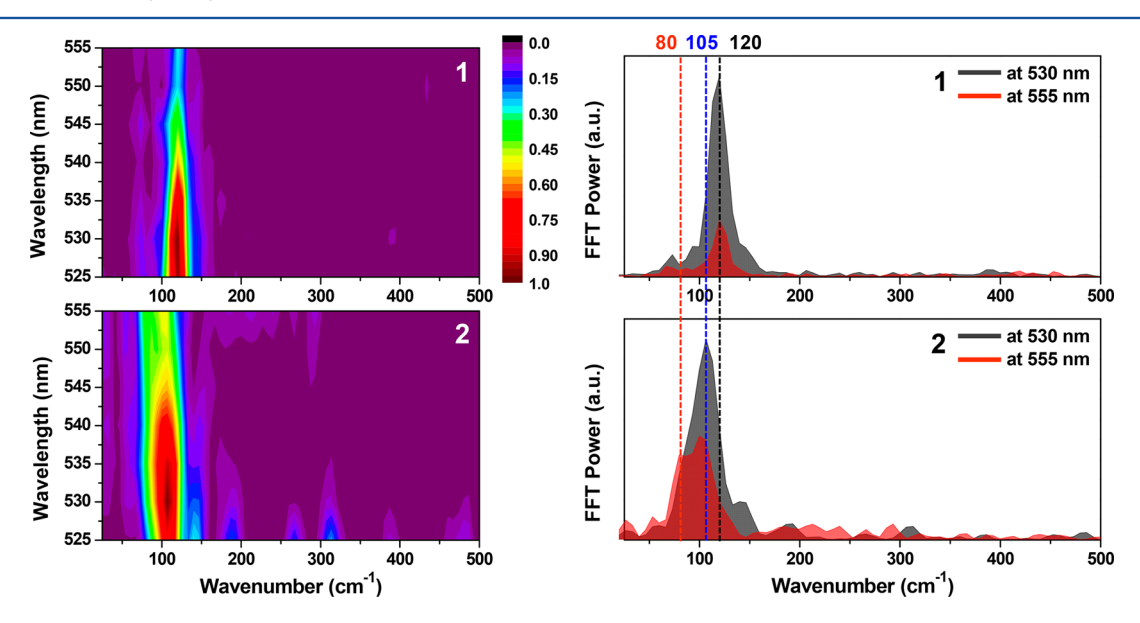


Figure 4. (Left) Contour map of Fourier power spectra below 500 cm<sup>-1</sup> as a function of the probe wavelength range of 525–555 nm. (Right) Fourier power spectra at specific probe wavelength of 530 and 555 nm. Vertical dashed line indicates the vibrational frequencies dominantly observed in the vibrational wavepacket dynamics of complexes 1 (black) and 2 (red and blue), respectively.

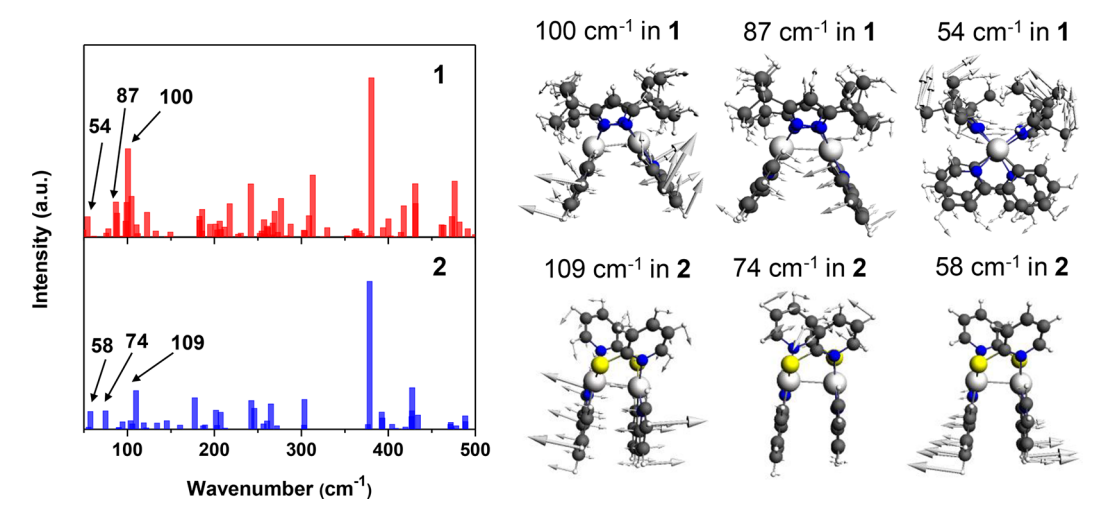


Figure 5. (Left) Frequencies of the normal modes in the ground-state calculated by DFT. Arrows indicate frequencies related to the Pt–Pt stretch vibration. (Right) Illustrations of the specific vibrational modes in 1 (at 54, 87, and 100 cm<sup>-1</sup>) and 2 (at 58, 74, and 109 cm<sup>-1</sup>) based on a ground-state DFT Raman frequency calculation.

calculated normal modes of the ground state geometry show the Pt-Pt stretching frequency increasing from 1 (100 cm<sup>-1</sup>) to 2 (109 cm<sup>-1</sup>), which is consistent with the results in the ground-state Raman measurements. Considering that the optimized ground-state molecular structures show a shorter Pt-Pt distance in 2 (2.872 Å) than in 1 (2.934 Å) as shown in Figure 6a, which closely matches results from the crystal structures, this feature follows the expected result where a higher force constant corresponds to a shorter Pt-Pt distance. However, the opposite occurs as the Pt-Pt stretching frequency downshifts for 2 (105 cm<sup>-1</sup>) compared to 1 (120 cm<sup>-1</sup>) in the vibrational wavepacket motions derived from the TA measurements. Moreover, the Fourier transform spectrum of 2 reveals quantitatively that the change of shapes as a function of the probe wavelength in the TA signals for 2 in Figure 2 originates from a lower frequency mode at  $\sim$ 80 cm<sup>-1</sup>, which is largely absent in 1. Taking the negative amplitude TA signals of 2 into account, one may consider the possibility of this frequency from the ground state Pt-Pt stretching, but such a rationale cannot explain why the amplitude of the higher frequency mode ( $\sim$ 120 cm<sup>-1</sup> in 1 and  $\sim$ 105 cm<sup>-1</sup> in 2) gradually decreases as the probe wavelength becomes longer and separates from the ground state bleaching, while the 80 cm<sup>-1</sup> component persists in 2 only. The ground-state Raman measurement in 2 exhibits one peak at ~96 cm<sup>-1</sup> below the Pt-Pt stretch vibration as shown in Figure S5, matching the vibrational modes at 58 or 74 cm<sup>-1</sup> in the normal mode spectra, which are related to cyclometalating (ppys) and the bridging ligands (pyts), respectively (Figure 5). This result suggests the vibrational frequency at ~80 cm<sup>-1</sup> in 2 comes from the vibrational motions localized on the ligands. In contrast, the vibrational wavepacket motion in 1 shows only one vibrational mode involving the Pt-Pt stretch, though two Raman peaks at ~72 and ~93 cm<sup>-1</sup> are observed in the ground-state Raman measurement (Figure S5), relating to the ligand vibrational modes at ~54 and ~87 cm<sup>-1</sup> in the normal modes spectrum (Figure 5). Collectively, the vibrational wavepacket motions in 1 and 2 suggest that the photoexcitation of the MMLCT state induces different structural changes in the excited state of 1 and

For a quantitative measure of the lifetime in the wavepacket motion, the oscillatory parts of the TA signals were each fit to a

cosine function for 1 and a superposition of two cosine functions with different parameters (amplitudes, phases, and periods) for 2, respectively, each superimposed with an exponential decay function with the dephasing time of the wavepacket motion (Figure 6b). The dephasing times for coherent wavepacket motions are extracted from the fits in a time window starting from ~350 fs to longer to avoid the coherent artifact around time zero, resulting in the coherence time of 705  $\pm$  56 fs for 1 and 340  $\pm$  40 fs for 2, respectively. It is worth noticing that the wavepacket of 2 displays a dephasing time two times faster than that of 1, which is consistent with the temporal behavior of TA kinetic traces, showing also two times faster decay traces in 2 ( $\sim$ 350 fs) than 1 ( $\sim$ 600 fs). Even though it is unclear whether the coherent vibrational motions in 1 and 2 come from the same TA signal (SE or ESA) or not, this feature shows the vibrational coherence time is closely related to the energy relaxation dynamics, supporting strongly that the vibrational wavepackets in 1 and 2 are generated in the excited state.

# DISCUSSION

Correlation between Molecular Geometry and Vibrational Wavepacket Motions. To explain the differences in coherent vibrational motions between 1 and 2, the ground state optimized structures of the two complexes are carefully examined (Figure 6a). Because the MMLCT transitions are dominated by the electronic transition from the Pt  $\sigma^*$  MO to the ligand  $\pi^*$  MOs, the structural parameters involving these two moieties in 1 and 2 are compared here. In addition to the already discussed differences in the ground state Pt-Pt distances, the other key structural difference is the shape of the molecule, "A" for 1 and "H" for 2, due to the different bridging groups connecting the two halves of the molecule, resulting in very different distances between the two  $\pi$ conjugated ligand planes. The center-to-center distance between the two ppy ligands in 1 is 5.64 Å, much longer than the range for normal  $\pi$ - $\pi$  nonbonding interactions. In contrast, the interligand distance in 2 is only 3.52 Å, well within the range of the  $\pi$ - $\pi$  nonbonding interactions in many conjugated organic materials. 41 Therefore, the energy levels of  $\pi^*$ -dominating MOs in 2 could be simultaneously modulated by the Pt-Pt stretching motions more than those in 1, resulting

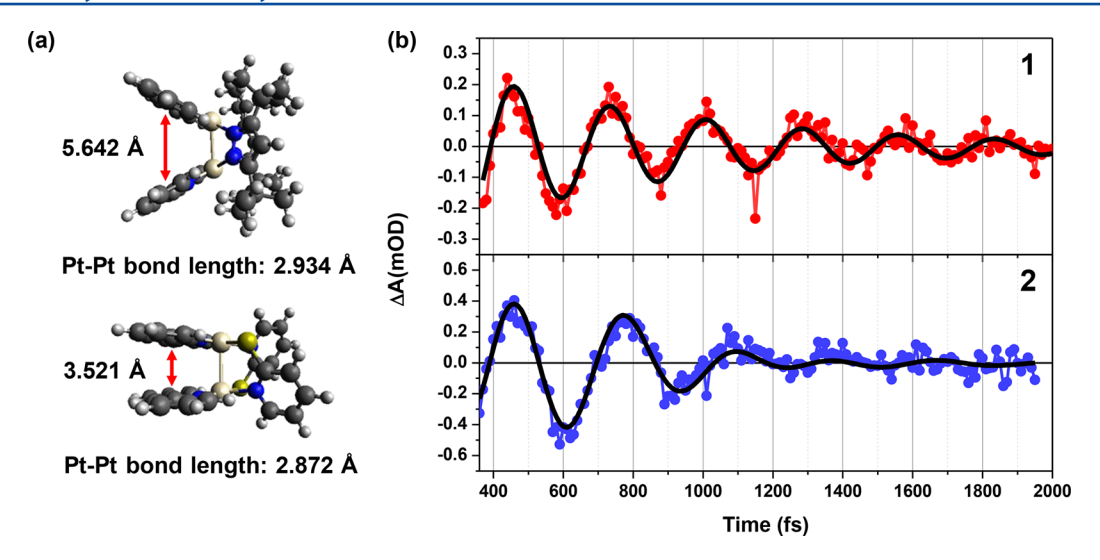


Figure 6. (a) Ball and stick representation of the optimized ground-state structure of 1 and 2. Arrows indicate the center-to-center distance between ppy ligand planes. (b) Oscillatory components of 1 and 2 observed at 540 nm after subtraction of the solvent contribution, together with the fit to exponentially damped cosine functions.

in stronger vibronic coupling of the ligand vibrational motions with the electronic transitions in 2. Inspired by our previous transient wide-angle X-ray scattering studies of 1 in solution, we found that ligand plane twisting can also be involved in the excited state molecular motions, and such a mode could have its own characteristic frequency on the same order.<sup>22</sup> In fact, the calculated Raman mode at 58 cm<sup>-1</sup> in 2 shows an intense transition with large-amplitude displacements in the distance between the ppy planes (Figure 5). Moreover, the features are consistent with a slight frequency downshift of the main peak assigned to the Pt-Pt stretching going from 1 to 2. The Pt-Pt stretch vibration in the Raman calculation in 1 and 2 shows that Pt-Pt stretching motion also accompanies the ligand plane bending to reduce the repulsion between them (Figure 5). Therefore, the shorter center-to-center distance between ppy ligands in 2 may lead to the modulation of Pt-Pt stretching frequency more than in 1.

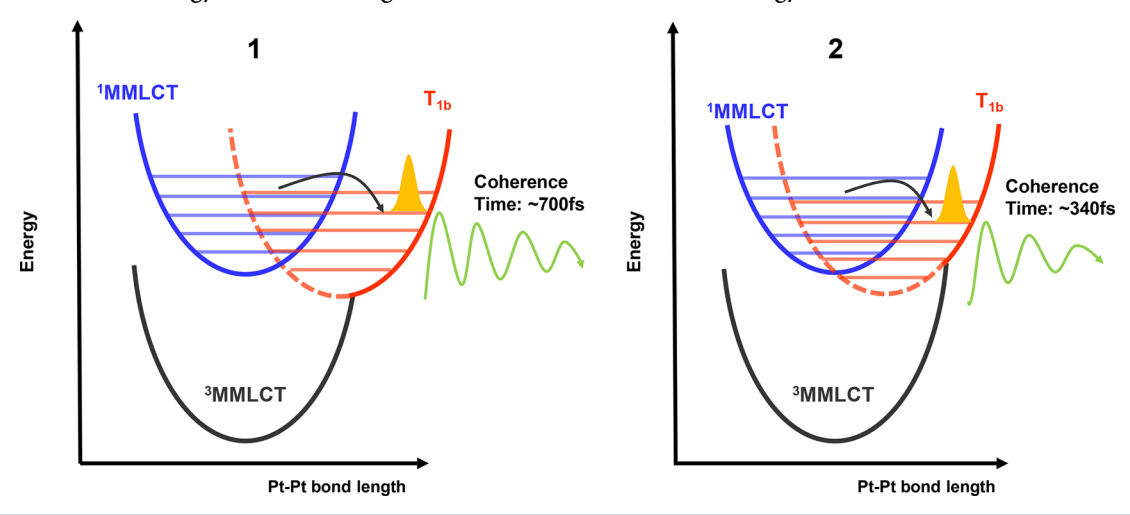
The previous study by Ma et al. reported that the intensity ratio between  $^3LC/MLCT$  and  $^3MMLCT$  states can be controlled also by the bulkiness of the cyclometalating ligand, which destabilizes the  $^3MMLCT$  state while the  $^3LC/MLCT$  state remains unaffected.  $^{24}$  This work showed that the steric interaction between cyclometalating ligands is another important factor to be considered in the contraction of Pt–Pt bond length in Pt(II) dimers. In this context, the different vibrational wavepacket motions between 1 and 2 show how  $\pi$ - $\pi$  interaction between the cyclometalating ligands impacts on the Pt–Pt contraction in the excited state of the Pt(II) dimer.

Vibrational Wavepacket Dynamics on Excited State Potential Energy Surfaces. To understand the physical meaning and implication of the observed coherent vibrational wavepacket dynamics in 1 and 2, we turn to the previous PES studies on similar Pt(II) dimers.<sup>23</sup> The theoretical work reported by Saito et al. demonstrated the coexistence of two triplet states,  $T_{1a}$  and  $T_{1b}$ , when calculated as a function of Pt–Pt distance. Saito et al. suggested that  $T_{1b}$ , the higher energy state with a minimum at a longer Pt–Pt distance, is an initial  $^3LC/MLCT$  state since its longer bond length mimics that of the ground state, while the  $T_{1a}$  state is the  $^3MMLCT$  state with the contraction discussed earlier. In our earlier calculations of

the PES as a function of the Pt-Pt distance for the derivatives of 1,32 we observed that, as the ground state Pt-Pt distance becomes shorter, the energy barrier for the internal conversion between the T<sub>1a</sub> and T<sub>1b</sub> states decreases and finally diminishes, stabilizing the <sup>3</sup>MMLCT state at a shorter Pt-Pt distance than that of the ground state as shown in Scheme 2. In each excited state trajectory on the PES, the previous work revealed four steps in the excited state energy cascade and relaxation processes for 1 and three of its derivatives in the same "A" frame structure but different Pt-Pt distances as the following: 46 (1) ultrafast ISC from the <sup>1</sup>MMLCT to the initial triplet T<sub>1b</sub> state within <200 fs (with IRF of ~200 fs), (2) the internal conversion from the  $T_{1b}$  to the <sup>3</sup>MMLCT state (2.6 ps), (3) vibrational cooling in <sup>3</sup>MMLCT state (73 ps), and (4) the ground state recovery (0.95  $\mu$ s). Here, the T<sub>1b</sub> state plays a very important role in the ultrafast ISC because the <sup>1</sup>MMLCT state becomes energetically closer to the T<sub>1b</sub> state as the Pt-Pt distance gets shorter in the ground state. In fact, various high z transition metal complexes including monomeric Pt(II) diamine complexes have shown that the triplet state is fully populated within 200 fs. 42–45 This phenomenon indicates that the ISC rate is not just governed by spin-orbit coupling strengths, but by the combination with other factors such as the existence of close-lying singlet or triplet states. 27,46 In addition, ultrafast ISC leads to preservation of the coherent vibrational wavepacket motion for some low vibrational modes even after ISC. Such an unusual feature has been observed in ultrafast TA studies of  $Cr(acac)_3$ ,  $^{47}$   $[Fe(bpy)_3]^{2+}$ ,  $^{48}$  a ruthenium-based supramolecular photocatalyst, 49 and other diplatinum complexes.<sup>27</sup> In fact, the ISC process here "filters" out those coherent wavepacket motions with much shorter period than the ISC time. The preserved vibrational wavepacket motions can also provide indirectly a time scale of the ISC process.

In addition, although the two calculations were not performed at the same level of theory, another theoretical work investigated the PES of 2, obtaining a similar shape and Pt—Pt distance in the triplet PES with those of 1.<sup>50</sup> Collectively, the distinct differences in coherent wavepacket motions between 1 and 2 can be understood in terms of such a triplet excited-state PES as depicted in Scheme 2. As the Pt—Pt distance in the ground state decreases from 1 to 2, the minima

Scheme 2. Schematic Energy Relaxation Diagram of 1 and 2 with Potential Energy Surfaces in Terms of Pt-Pt Distance



of the two triplet surfaces in 2 approach each other along the reaction coordinate more than in 1. In this sense, the two PES parabolas in 2 become nested more than those in 1, resulting in a shorter time for the internal conversion in 2 along a cascade pathway from  $T_{1b}$  to  $^3$ MMLCT state. Therefore, if the vibrational coherence comes from  $T_{1b}$  state by ultrafast ISC, the difference in the shape of the PES between 1 and 2 results in a shorter-lived vibrational coherence in 2 than in 1 as in Figure 6b. This assumes that internal conversion from  $T_{1b}$  to  $^3$ MMLCT accompanies the Pt–Pt distance shortening that ultimately destroys the vibrational coherence. Furthermore, in this mechanism, the observation of ligand vibrational modes in 2 suggests that Pt–Pt contraction during the internal conversion is strongly correlated with the  $\pi$ - $\pi$  interaction between ppy ligands.

Even though this study does not reveal directly the occurrence of ultrafast ISC, we believe the dependence of vibrational wavepacket dynamics on the molecular geometry provides considerable credibility to the notion that the interaction between cyclometalating ligands in Pt(II) dimers is a very important factor in the Pt–Pt contraction as well as the energy relaxation dynamics. In the future, ultrafast broadband TA experiments will be performed to further confirm the ultrafast ISC and the excited-state wavepacket motion involving the molecular structural transformation. Furthermore, a femtosecond X-ray scattering experiment will be carried out soon to track the ultrafast excited state pathway using the Pt–Pt distance evolution as a probe to map out the excited state PES and excited state trajectory.

# CONCLUSION

In this work, we investigated the vibrational wavepacket dynamics in cyclometalated Pt(II) dimers that have different molecular geometries by using ultrafast degenerate TA spectroscopy and theoretical calculations. Although the current TA experiments did not reveal directly the ISC rate due to the strong coherent spike and oscillations at short times, both complexes 1 and 2 clearly showed very strong coherent oscillations related to Pt–Pt stretching motion by photoexcitation of the <sup>1</sup>MMLCT state. Interestingly, the vibrational wavepacket in 2 exhibited multiple frequencies at 80 and 105 cm<sup>-1</sup>, which are downshifted from the single frequency of 120 cm<sup>-1</sup> in 1. Based on the optimized ground state structure and

the Raman calculations, the features are very closely correlated with "H" framed geometry in 2 compared to the "A" frame in 1, leading to the sharply increased  $\pi - \pi$  interaction between ppy ligands, resulting in strong vibronic coupling of ligand vibrational modes with the MMLCT transitions as well as modulation of the Pt-Pt stretching frequency. Furthermore, the shorter coherence time in 2 indicates the triplet PES in 2 narrows relative to 1, which is consistent with the previously proposed triplet PES model. Collectively, the finding herein suggests that interaction between cyclometalating ligands may be a key factor in determining the Pt-Pt contraction and the related energy relaxation dynamics in the Pt(II) dimers. In conclusion, this work demonstrates that the coherent vibrational wavepacket provides new insight into the photoinduced structural changes of diplatinum complexes, which is crucial for development of the transition metal-based systems for OLED technologies.

#### ASSOCIATED CONTENT

## S Supporting Information

The Supporting Information is available free of charge on the ACS Publications website at DOI: 10.1021/acs.jpcc.8b01636.

Contour plot of the transient grating signal of the optimally compressed pulses and intensity profile probed at 535 nm used in all TA measurements, magic-angle TA kinetics traces at several probe wavelengths in THF, reconstructed magic-angle TA kinetics traces, Fourier power spectra below 1200 cm<sup>-1</sup> at 530 nm in THF and toluene, and solid powder Raman spectra (PDF)

# AUTHOR INFORMATION

#### ORCID ®

Richard P. Van Duyne: 0000-0001-8861-2228 George C. Schatz: 0000-0001-5837-4740 Felix N. Castellano: 0000-0001-7546-8618 Lin X. Chen: 0000-0002-8450-6687

# Notes

The authors declare no competing financial interest.

# ACKNOWLEDGMENTS

This work has been supported by funding by the Ultrafast Initiative of the U.S. Department of Energy, Office of Science, Office of Basic Energy Sciences, through Argonne National Laboratory under Contract No. DE-AC02-06CH11357 and from the National Science Foundation (CHE-1363007 to L.X.C. and CHE-1362942 to F.N.C.). The computational work is supported by the U.S. Department of Energy, Office of Science, Office of Basic Energy Sciences, under Contract No. DE-AC02-06CH11357. M.S.K. would like to acknowledge his NDSEG fellowship sponsored by the Air Force Office of Scientific Research.

#### REFERENCES

- (1) Evans, R. C.; Douglas, P.; Winscom, C. J. Coordination Complexes Exhibiting Room-Temperature Phosphorescence: Evaluation of Their Suitability as Triplet Emitters in Organic Light Emitting Diodes. *Coord. Chem. Rev.* **2006**, *250*, 2093–2126.
- (2) Ma, B.; Djurovich, P. I.; Garon, S.; Alleyne, B.; Thompson, M. E. Platinum Binuclear Complexes as Phosphorescent Dopants for Monochromatic and White Organic Light-Emitting Diodes. *Adv. Funct. Mater.* **2006**, *16*, 2438–2446.
- (3) Gareth Williams, J. A.; Develay, S.; Rochester, D. L.; Murphy, L. Optimising the Luminescence of Platinum(II) Complexes and Their Application in Organic Light Emitting Devices(OLEDs). *Coord. Chem. Rev.* 2008, 252, 2596–2611.
- (4) Ho, C.-L.; Wong, W.-Y.; Yao, B.; Xie, Z.; Wang, L.; Lin, Z. Synthesis, Characterization, Photophysics and Electrophosphorescent Applications of Phosphorescent Platinum Cyclometalated Complexes with 9-Arylcarbazole Moieties. *J. Organomet. Chem.* **2009**, 694, 2735–2749
- (5) Wang, K.-W.; Chen, J.-L.; Cheng, Y.-M.; Chung, M.-W.; Hsieh, C.-C.; Lee, G.-H.; Chou, P.-T.; Chen, K.; Chi, Y. Mono- Versus Dinuclear Pt(II) 6-(5-Trifluoromethyl-Pyrazol-3-yl)-2,2'-Bipyridine Complexes: Synthesis, Characterization, and Remarkable Difference in Luminescent Properties. *Inorg. Chem.* **2010**, *49*, 1372–1383.
- (6) Fleetham, T.; Ecton, J.; Wang, Z.; Bakken, N.; Li, J. Single-Doped White Organic Light-Emitting Device with an External Quantum Efficiency over 20%. *Adv. Mater.* **2013**, *25*, 2573–2576.
- (7) Po, C.; Ke, Z.; Tam, A. Y. Y.; Chow, H. F.; Yam, V. W. W. A Platinum(II) Terpyridine Metallogel with an L-Valine-Modified Alkynyl Ligand: Interplay of Pt···Pt,  $\pi$ – $\pi$  and Hydrogen-Bonding Interactions. *Chem. Eur. J.* **2013**, *19*, 15735–15744.
- (8) Leung, S. Y.-L.; Evariste, S.; Lescop, C.; Hissler, M.; Yam, V. W.-W. Supramolecular Assembly of a Phosphole-Based Moiety into Nanostructures Dictated by Alkynylplatinum(II) Terpyridine Complexes through Non-Covalent Pt···Pt And  $\pi-\pi$  Stacking Interactions: Synthesis, Characterization, Photophysics and Self-Assembly Behaviors. *Chemical Science* **2017**, *8*, 4264–4273.
- (9) Gray, H. B.; Záliš, S.; Vľček, A. Electronic Structures and Photophysics of d<sub>8</sub>-d<sub>8</sub> Complexes. *Coord. Chem. Rev.* **2017**, 345, 297–317.
- (10) Ma, B.; Li, J.; Djurovich, P. I.; Yousufuddin, M.; Bau, R.; Thompson, M. E. Synthetic Control of Pt···Pt Separation and Photophysics of Binuclear Platinum Complexes. *J. Am. Chem. Soc.* **2005**, 127, 28−29.
- (11) Rachford, A. A.; Castellano, F. N. Thermochromic Absorption and Photoluminescence in  $[Pt(ppy)(\mu-Ph_2pz)]_2$ . *Inorg. Chem.* **2009**, 48, 10865–10867.
- (12) Chakraborty, A.; Deaton, J. C.; Haefele, A.; Castellano, F. N. Charge-Transfer and Ligand-Localized Photophysics in Luminescent Cyclometalated Pyrazolate-Bridged Dinuclear Platinum(II) Complexes. *Organometallics* **2013**, 32, 3819–3829.
- (13) Han, M.; Tian, Y.; Yuan, Z.; Zhu, L.; Ma, B. A Phosphorescent Molecular "Butterfly" that Undergoes a Photoinduced Structural Change Allowing Temperature Sensing and White Emission. *Angew. Chem., Int. Ed.* **2014**, *53*, 10908–10912.
- (14) Zhou, C.; Yuan, L.; Yuan, Z.; Doyle, N. K.; Dilbeck, T.; Bahadur, D.; Ramakrishnan, S.; Dearden, A.; Huang, C.; Ma, B. Phosphorescent Molecular Butterflies with Controlled Potential-

- Energy Surfaces and Their Application as Luminescent Viscosity Sensor. *Inorg. Chem.* **2016**, *55*, 8564–8569.
- (15) Kim, C. D.; Pillet, S.; Wu, G.; Fullagar, W. K.; Coppens, P. Excited-State Structure by Time-Resolved X-Ray Diffraction. *Acta Crystallogr., Sect. A: Found. Crystallogr.* **2002**, *58*, 133–137.
- (16) Christensen, M.; Haldrup, K.; Bechgaard, K.; Feidenhans'l, R.; Kong, Q.; Cammarata, M.; Russo, M. L.; Wulff, M.; Harrit, N.; Nielsen, M. M. Time-Resolved X-Ray Scattering of an Electronically Excited State in Solution. Structure of the <sup>3</sup>A<sub>2u</sub> State of Tetrakis- $\mu$ -Pyrophosphitodiplatinate(II). *J. Am. Chem. Soc.* **2009**, *131*, 502–508.
- (17) Haldrup, K.; Christensen, M.; Nielsen, M. M. Analysis of Time-Resolved X-Ray Scattering Data from Solution-State Systems. *Acta Crystallogr., Sect. A: Found. Crystallogr.* **2010**, *66*, 261–269.
- (18) Novozhilova, I. V.; Volkov, A. V.; Coppens, P. Theoretical Analysis of the Triplet Excited State of the [Pt<sub>2</sub>(H<sub>2</sub>P<sub>2</sub>O<sub>5</sub>)<sub>4</sub>]<sup>4</sup> Ion and Comparison with Time-Resolved X-Ray and Spectroscopic Results. *J. Am. Chem. Soc.* **2003**, 125, 1079–1087.
- (19) Van Der Veen, R. M.; Milne, C. J.; El Nahhas, A.; Lima, F. A.; Pham, V. T.; Best, J.; Weinstein, J. A.; Borca, C. N.; Abela, R.; Bressler, C.; Chergui, M. Structural Determination of a Photochemically Active Diplatinum Molecule by Time-Resolved EXAFS Spectroscopy. *Angew. Chem., Int. Ed.* **2009**, *48*, 2711–2714.
- (20) Haldrup, K.; Christensen, M.; Cammarata, M.; Kong, Q.; Wulff, M.; Mariager, S. O.; Bechgaard, K.; Feidenhans'l, R.; Harrit, N.; Nielsen, M. M. Structural Tracking of a Bimolecular Reaction in Solution by Time-Resolved X-Ray Scattering. *Angew. Chem., Int. Ed.* **2009**, *48*, 4180–4184.
- (21) Chergui, M. Ultrafast Photophysics of Transition Metal Complexes. *Acc. Chem. Res.* **2015**, *48*, 801–808.
- (22) Haldrup, K.; Dohn, A. O.; Shelby, M. L.; Mara, M. W.; Stickrath, A. B.; Harpham, M. R.; Huang, J.; Zhang, X.; MØLler, K. B.; Chakraborty, A.; Castellano, F. N.; Tiede, D. M.; Chen, L. X. Butterfly Deformation Modes in a Photoexcited Pyrazolate-Bridged Pt Complex Measured by Time-Resolved X-Ray Scattering in Solution. *J. Phys. Chem. A* 2016, 120, 7475–7483.
- (23) Saito, K.; Nakao, Y.; Sakaki, S. Theoretical Study of Pyrazolate-Bridged Dinuclear Platinum(II) Complexes: Interesting Potential Energy Curve of the Lowest Energy Triplet Excited State and Phosphorescence Spectra. *Inorg. Chem.* **2008**, *47*, 4329–4337.
- (24) Zhou, C.; Tian, Y.; Yuan, Z.; Han, M.; Wang, J.; Zhu, L.; Tameh, M. S.; Huang, C.; Ma, B. Precise Design Of Phosphorescent Molecular Butterflies with Tunable Photoinduced Structural Change and Dual Emission. *Angew. Chem., Int. Ed.* **2015**, *54*, 9591–9595.
- (25) Roundhill, D. M.; Gray, H. B.; Che, C. M. Pyrophosphito-Bridged Diplatinum Chemistry. Acc. Chem. Res. 1989, 22, 55–61.
- (26) Van Der Veen, R. M.; Cannizzo, A.; Van Mourik, F.; Vlček, A.; Chergui, M. Vibrational Relaxation and Intersystem Crossing of Binuclear Metal Complexes in Solution. *J. Am. Chem. Soc.* **2011**, *133*, 305–315.
- (27) Monni, R.; Auböck, G.; Kinschel, D.; Aziz-Lange, K. M.; Gray, H. B.; Vlček, A.; Chergui, M. Conservation of Vibrational Coherence in Ultrafast Electronic Relaxation: the Case of Diplatinum Complexes in Solution. *Chem. Phys. Lett.* **2017**, *683*, 112–120.
- (28) Lingerfelt, D. B.; Lestrange, P. J.; Radler, J. J.; Brown-Xu, S. E.; Kim, P.; Castellano, F. N.; Chen, L. X.; Li, X. Can Excited State Electronic Coherence be Tuned via Molecular Structural Modification? A First-Principles Quantum Electronic Dynamics Study of Pyrazolate-Bridged Pt(II) Dimers. J. Phys. Chem. A 2017, 121, 1932—1939.
- (29) Koshiyama, T.; Omura, A.; Kato, M. Redox-Controlled Luminescence of a Cyclometalated Dinuclear Platinum Complex Bridged with Pyridine-2-Thiolate Ions. *Chem. Lett.* **2004**, *33*, 1386–1387.
- (30) Lockard, J. V.; Rachford, A. A.; Smolentsev, G.; Stickrath, A. B.; Wang, X.; Zhang, X.; Atenkoffer, K.; Jennings, G.; Soldatov, A.; Rheingold, A. L.; Castellano, F. N.; Chen, L. X. Triplet Excited State Distortions in a Pyrazolate Bridged Platinum Dimer Measured by X-Ray Transient Absorption Spectroscopy. *J. Phys. Chem. A* **2010**, *114*, 12780–12787.

- (31) Cho, S.; Mara, M. W.; Wang, X.; Lockard, J. V.; Rachford, A. A.; Castellano, F. N.; Chen, L. X. Coherence In Metal—Metal-to-Ligand-Charge-Transfer Excited States of a Dimetallic Complex Investigated by Ultrafast Transient Absorption Anisotropy. *J. Phys. Chem. A* **2011**, *115*, 3990—3996.
- (32) Brown-Xu, S. E.; Kelley, M. S. J.; Fransted, K. A.; Chakraborty, A.; Schatz, G. C.; Castellano, F. N.; Chen, L. X. Tunable Excited-State Properties and Dynamics as a Function of Pt–Pt Distance in Pyrazolate-Bridged Pt(II) Dimers. *J. Phys. Chem. A* **2016**, *120*, 543–550
- (33) Fonseca Guerra, C.; Snijders, J. G.; Te Velde, G.; Baerends, E. J. Towards an Order-N DFT Method. *Theor. Chem. Acc.* **1998**, *99*, 391–403
- (34) te Velde, G.; Bickelhaupt, F. M.; Baerends, E. J.; Guerra, C. F.; Gisbergen, S. J. A. V.; Snijders, J. G.; Ziegler, T. Chemistry with ADF. *J. Comput. Chem.* **2001**, *22*, 931–967.
- (35) Baerends, E. J.; Ziegler, T.; Atkins, A. J.; Autschbach, J.; Bashford, D.; Bérces, A.; Bickelhaupt, F. M.; Bo, C.; Boerritger, P. M.; Cavallo, L. et al. *ADF2016*; SCM, Theoretical Chemistry, Vrije Universiteit: Amsterdam, The Netherlands. https://www.scm.com.
- (36) Lenthe, E. V.; Baerends, E. J.; Snijders, J. G. Relativistic Regular Two-Component Hamiltonians. J. Chem. Phys. 1993, 99, 4597–4610.
- (37) van Lenthe, E.; Baerends, E. J.; Snijders, J. G. Relativistic Total Energy using Regular Approximations. *J. Chem. Phys.* **1994**, *101*, 9783–9792.
- (38) van Lenthe, E.; Ehlers, A.; Baerends, E.-J. Geometry Optimizations in the Zero Order Regular Approximation for Relativistic Effects. *J. Chem. Phys.* **1999**, *110*, 8943–8953.
- (39) Abraham, B.; Nieto-Pescador, J.; Gundlach, L. Ultrafast Relaxation Dynamics of Photoexcited Zinc-Porphyrin: Electronic-Vibrational Coupling. *J. Phys. Chem. Lett.* **2016**, *7*, 3151–3156.
- (40) Kapitan, J.; Hecht, L.; Bour, P. Raman Spectral Evidence of Methyl Rotation in Liquid Toluene. *Phys. Chem. Chem. Phys.* **2008**, *10*, 1003–1008.
- (41) Hunter, C. A.; Sanders, J. K. M. The Nature of  $\pi$ - $\pi$  Interactions. *J. Am. Chem. Soc.* **1990**, *112*, 5525–5534.
- (42) Juban, E. A.; Smeigh, A. L.; Monat, J. E.; Mccusker, J. K. Ultrafast Dynamics of Ligand-Field Excited States. *Coord. Chem. Rev.* **2006**, 250, 1783–1791.
- (43) Ramakrishna, G.; Goodson, T.; Rogers-Haley, J. E.; Cooper, T. M.; Mclean, D. G.; Urbas, A. Ultrafast Intersystem Crossing: Excited State Dynamics of Platinum Acetylide Complexes. *J. Phys. Chem. C* **2009**, *113*, 1060–1066.
- (44) Danilov, E. O.; Pomestchenko, I. E.; Kinayyigit, S.; Gentili, P. L.; Hissler, M.; Ziessel, R.; Castellano, F. N. Ultrafast Energy Migration in Platinum(II) Diimine Complexes Bearing Pyrenylacetylide Chromophores. *J. Phys. Chem. A* **2005**, *109*, 2465–2471.
- (45) Glik, E. A.; Kinayyigit, S.; Ronayne, K. L.; Towrie, M.; Sazanovich, I. V.; Weinstein, J. A.; Castellano, F. N. Ultrafast Excited State Dynamics of Pt(II) Chromophores Bearing Multiple Infrared Absorbers. *Inorg. Chem.* **2008**, *47*, 6974–6983.
- (46) Cannizzo, A.; Blanco-Rodríguez, A. M.; El Nahhas, A.; Šebera, J.; Záliš, S.; Vlček, A.; Chergui, M. Femtosecond Fluorescence and Intersystem Crossing in Rhenium(I) Carbonyl—Bipyridine Complexes. J. Am. Chem. Soc. 2008, 130, 8967—8974.
- (47) Schrauben, J. N.; Dillman, K. L.; Beck, W. F.; Mccusker, J. K. Vibrational Coherence in the Excited State Dynamics of Cr(Acac)<sub>3</sub>: Probing the Reaction Coordinate for Ultrafast Intersystem Crossing. *Chemical Science* **2010**, *1*, 405–410.
- (48) Auböck, G.; Chergui, M. Sub-50-fs Photoinduced Spin Crossover in [Fe(Bpy)<sub>3</sub>]<sup>2+</sup>. *Nat. Chem.* **2015**, *7*, 629.
- (49) Wächtler, M.; Guthmuller, J.; Kupfer, S.; Maiuri, M.; Brida, D.; Popp, J.; Rau, S.; Cerullo, G.; Dietzek, B. Ultrafast Intramolecular Relaxation and Wave-Packet Motion in a Ruthenium-Based Supramolecular Photocatalyst. *Chem. Eur. J.* **2015**, *21*, 7668–7674.
- (50) Saito, K.; Nakao, Y.; Umakoshi, K.; Sakaki, S. Theoretical Study of Excited States of Pyrazolate- and Pyridinethiolate-Bridged Dinuclear Platinum(II) Complexes: Relationship Between Geometries of Excited

States and Phosphorescence Spectra. Inorg. Chem. 2010, 49, 8977-8985